Limitations of soil moisture and formation rate on vegetation growth in karst areas

Sirui Zhang [a,b], Xiaoyong Bai [a,b,d,*], Cuiwei Zhao [b], Qiu Tan [b], Guangjie Luo [e], Yue Cao [a,c], Yuanhong Deng [a,c], Qin Li [a,c], Chaojun Li [a], Luhua Wu [a,c], Jinfeng Wang [a,f], Fei Chen [a,f], Huipeng Xi [a,c], Chen Ran [a,b], Min Liu [a,b]

[a] State Key Laboratory of Environmental Geochemistry, Institute of Geochemistry, Chinese Academy of Sciences, Guiyang 550081, China
[b] School of Geography and Environmental Sciences, Guizhou Normal University, Guiyang 550001, Guizhou Province, China
[c] Puding Karst Ecosystem Observation and Research Station, Chinese Academy of Sciences, Puding 562100, China
[d] CAS Center for Excellence in Quaternary Science and Global Change, Xi'an 710061, Shanxi Province, China
[e] Guizhou Provincial Key Laboratory of Geographic State Monitoring of Watershed, Guizhou Education University, Guiyang 550018, China
[f] College of Resources and Environmental Engineering, Guizhou University, Guiyang 550025, China

HIGHLIGHTS

- The spatial map ($0.125° \times 0.125°$) of the global karst ecosystem with a static/dynamic limitation zone was established.
- The global karst ecosystem was jointly limited by SFR and SM.
- 25.15 t km^{-2} yr^{-1} and 0.276 m^3 m were the ecological thresholds of the SFR and SM, respectively.
- The SFR limitation on vegetation was mainly concentrated in Boreal forest (17%).
- The current state of SFR and SM may make large areas of karst tropical rainforest facing degradation into a savanna.

GRAPHICAL ABSTRACT
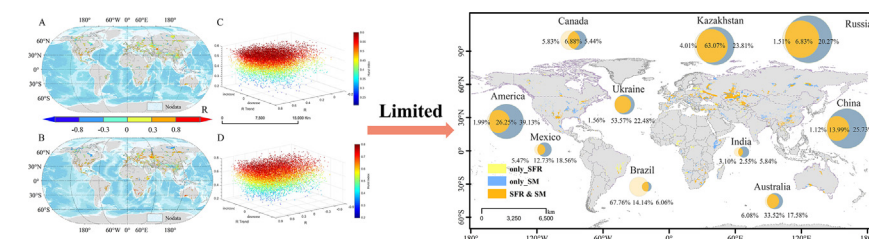
ARTICLE INFO

ABSTRACT

Vegetation changes in karst areas are controlled by the soil formation rate (SFR) and soil moisture (SM). However, little is known about their thresholds and global control patterns. To this end, based on high-precision climate and vegetation data for 2000–2014, using Pearson correlation analysis, the Hurst index, and change-point analysis, the thresholds of the SFR and SM in vegetation growth in karst areas were identified. Furthermore, a spatial map ($0.125° \times 0.125°$) of the global karst ecosystem with a static/dynamic limitation zone was established. We found that the net primary productivity (NPP) in 70% of the global climate zones exhibited a dual restriction relationship with the SM and SFR. The limitations of the SFR and SM in vegetation growth were most obvious in subpolar and semi-arid climates. In addition, their ecological thresholds were 25.2 t km^{-2} yr^{-1} and 0.28 m^3 m^{-3}, respectively. The static limitation of the SFR on the NPP in karst areas accounted for 28.37%, and the influence of the SM enhanced this limit (21.79%). The limitation of the SFR on vegetation was mainly concentrated in Boreal forests (17%), and the limitation of the SM was mainly concentrated in tropical savannas (12%). The NPP and the Normalized Difference Vegetation Index (NDVI) were the most sensitive to changes in the SM and SFR. Moreover, the analysis based on 14 ecologically limitation karst areas further revealed that the reduction in these factors may cause the tropical rain forest to experience degradation. It can be seen that the SM enhanced

* Corresponding author at: State Key Laboratory of Environmental Geochemistry, Institute of Geochemistry, Chinese Academy of Sciences, 99 Lincheng West Road, Guiyang 550081, Guizhou Province, China.
E-mail address: baixiaoyong@vip.skleg.cn (X. Bai).

the limiting effect of the SFR on vegetation in karst areas. In short, this interpretation of karst vegetation limitations provides a deeper understanding of and approach to ecosystem evolution and vegetation restoration in these regions.

1. Introduction

As the climate warms, the functions of terrestrial ecosystems are strongly promoted under the effect of global CO_2 fertilization, especially in mid-to-high latitude regions (Idso and Kimball, 1993; Nemani et al., 2003; Silva and Lambers, 2018). However, several studies have found that the rising atmospheric CO_2 concentration rarely translates into increased vegetation growth (VG) in natural ecosystems (Oren et al., 2001; Dolan et al., 2017). To achieve the healthy development of the ecosystem and the restoration of vegetation, it is necessary to understand the internal response of this phenomenon. Soil moisture (SM) plays a key role in global climate change and represents the precipitation and radiation anomalies (Seneviratne et al., 2010). In regard to the forest ecosystem, the dynamic characteristics of the SM are of great significance to understanding the development process, element migration, and material circulation in the soil and the relationship between these factors and VG (Cowling et al., 1997; Kidron, 2000; Lu et al., 2017). Therefore, as an important non-biological limiting factor of the ecological pattern, the SM determines the type, quantity, and distribution of the vegetation (Liu et al., 2020). In addition to the SM, the soil developed through chemical weathering of the original bedrock is also the main source of mineral nutrients required for VG (Kidron, 2000; Silva and Lambers, 2018), and thus, it regulates the growth potential of plants and soil carbon saturation (Jiang et al., 2020; Yan et al., 2019).

In karst areas, especially in hot and humid areas, soil formation is dominated by chemical weathering (Stockmann et al., 2014), but the carbonate rocks in these areas are inherently deficient in soil material (low carbonate rock acidic insoluble matter content) (Cao et al., 2017; Wu and Qi, 2021). Therefore, the growth of karst vegetation is limited by the geological background (Jiang et al., 2020), which is mainly reflected in the low rate of soil formation (Yuan, 1988), the barren soil layer, and the differences in the soil loss mechanisms in karst and non-karst areas. Their characteristics affect the SM and soil fertility and have an important restrictive effect on the formation and evolution of ecosystems in karst areas. It is difficult for the vegetation in karst areas to form a dense vegetation cover, and the ecosystem is fragile (Li et al., 2020). Many studies have focused on the spatial patterns of forest communities and have demonstrated that the forests in karst areas are significantly affected by the soil fertility (Zhang et al., 2021b). Although soil nutrients are largely dependent on the soil formation rate (SFR) under the special geological environmental conditions (Zhang et al., 2021a), research on the SFR and its effect on the environment is quite weak. Moreover, many soil studies have been based on locations or local areas; so, there is a lack of soil studies based on large-scale areas (Amundson, 2021). The impact of the interactions between the soil and vegetation in karst areas on the global environment remains unpredictable. In addition, it has also largely limited the in-depth study of a series of resources and environmental issues in this filed.

In this study, we comprehensively considered the SFR and SM in karst areas and selected the net primary productivity (NPP), Normalized Difference Vegetation Index (NDVI), tree height (TH), and vegetation richness (VR) as VG indicators in order to clarify the response of vegetation to typical karst environmental factors (SFR and SM). By determining the common limitations of the SFR and SM on vegetation, their thresholds for vegetation in different ecological regions were determined. Finally, the key areas of the spatial static/dynamic limitations were identified. The results of this study link the distribution of plant

traits with soil environmental characteristics and geochemical processes. These results provide valuable information for understanding the interaction mechanism between vegetation and the soil environment in karst areas and allow us to predict changes in ecosystem functions for use in global environmental governance.

2. Materials and methods

2.1. Different indicator datasets

The NPP and the NDVI data of the global karst areas are respectively derived from Moderate-resolution Imaging Spectroradiometer (MODIS) datasets including MOD17A3 and MOD13A3 of National Aeronautics and Space Administration (NASA)/EOS LPDAAC Data Distribution Center (https://earthdata.nasa.gov/), with a spatial resolution of 1 km and a time span of 2000–2014. Then, the data were converted into Albers projection, stitching, cropping and other processing by using the professional processing software (MRT TOOLS) provided by MODIS website to project. We further analyzed the relationship with different the NPP data and soil in order to more fully verify the reliability of the results of this manuscript. These data include (1) the NPP data based on the Carnegie-Ames-Stanford approach (CASA) model from NASA (https://earthdata.nasa.gov/); (2) the NPP data based on the Integrated Biosphere Simulator (IBIS) model, and it has been extensively verified (Zhang et al., 2013); (3) the NPP data based on the Light Use Efficiency model, and it was verified using FLUXNET site data. The accuracy of the algorithm was $R^2 = 0.559$, RMSE = 2.782 gC/m^{2}d (Wang et al., 2020b).

In this study, the Geoscience Laser Altimeter System (GLAS) was used to retrieve the vegetation TH data (Simard et al., 2011) based on the Ice, Cloud, and Land Elevation Satellite (ICESat) launched by the National Aeronautics and Space Administration (NASA) in 2003. Compared with similar existing data, the data are more consistent with the verification data and have a good regional practicability (Lefsky, 2010). Finally, the spatial data (Kreft and Jetz, 2007) on the vascular plant richness were obtained from Kreft and Jetz's global dataset of 1032 geographic region units in 2007. The above datasets have been widely used to study global vegetation, and they are also applicable to karst ecosystems (Gonsamo et al., 2016; Bai et al., 2019). The climate data were obtained from NASA (https://disc.gsfc.nasa.gov), including the global daily precipitation, temperature, evaporation, and solar radiation data from 2000 to 2014, and monthly data were synthesized from these datasets. The reliability of all of the data has been recognized by other researchers (Qiu et al., 2014; Deng et al., 2020a, 2020b). In addition, in this study, the European Centre for Medium-Range Weather Forecasts Re-Analysis-Interim (ERA-INTERM) SM data were obtained from the European medium-sized weather forecast center (https://www.ecmwf.int/). The monthly range is 0.125°, and the soil depth that is regarded as the global surface is 0–7 cm. The HCO_3^- and CA^{2+} ion concentration data were derived from the GLORICH-Global river chemistry database (Hartmann et al., 2019). This database contains information from more than 1.27 million samples and 18,000 sampling locations. In this study, 15,517 ion concentration monitoring data from different regions were screened. The carbonate outcrop area was determined from the carbonate outcrop world map provided by the University of Auckland (http://www.sges.auckland.ac.nz/sges_research/karst.shtm). The boundary was also included in the data. This includes regional boundaries in more detail.

2.2. Global boundaries datasets

In order to better link spatial information to specific regions, this study used different types of regional divisions for the world. Among them, global national vector boundary data (https://gadm.org/) and Köppen climate zone classification data (Finlayson and Mcmahon, 2007) were used. At the same time, in the process of quantifying the ecological threshold of SM and SFR on vegetation, the irrelevant variables should be control as much as possible. Therefore this study used global ecological region distribution data (Olson et al., 2001).

2.3. Estimation of SFR

Based on the equilibrium reaction of calcite dissolution, Gombert (2002) established a carbonate rock theory maximum potential dissolution (MPD) calculation model by assuming that the carbonate rock dissolution reaction reaches equilibrium. The formula is as follows:

$$D_{\max} = 10^6(P-E)\left[Ca^{2+}\right]_{eq}$$
$$= 10^6(P-E)\left(K_S K_1 K_0/4K_2 \gamma_{Ca^{2+}} \gamma_{(HCO_3^-)}{}^2\right)^{1/3} (pCO_2)^{1/3} \quad (1)$$

where P and E are the average annual precipitation and evapotranspiration, respectively. K_s, K_1, K_0, and K_2 are the calcite solubility constant and the equilibrium constants when CO_2 is converted into HCO_3^-, dissolved in water, and converted into CO_3^{2-}. Additionally, γi is the activity coefficient of ion i in water, and pCO_2 is the partial pressure of CO_2.

The SFR in karst areas can be calculated using the MPD model (Li et al., 2020):

$$T = vQ\rho P + R(1-)P \quad (2)$$

where v is the dissolution rate of the carbonate rock (m^3 km^{-2} yr^{-1}); Q and P are the acid-insoluble content (%) and carbonate rock content (%), respectively; ρ is the density of limestone under laboratory conditions (t m^{-3}); and R is the SFR of non-carbonate rocks (t km^{-2} yr^{-1}).

2.4. Change - point analysis

This study used Change-point analyzer 2.3 (Taylor Enterprises, USA) to detect and analyze the relationship with vegetation indicators (VIs) and the SFR and the SM. Then, the SFR and the SM thresholds corresponding to the quantitative characteristics of different plant communities were determined.

2.5. Pearson correlation analysis

Pearson correlation coefficient was used for correlation analyses between which the annual average the VIs of each pixel and the SFR and the SM, the response between them was clarified. The calculation formula is:

$$R = \frac{\sum\limits_{i=1}^{n}(x_i-\overline{x})(y_i-\overline{y})}{\sqrt{\sum\limits_{i=1}^{n}(x_i-\overline{x})^2 \sum\limits_{i=1}^{n}(y_i-\overline{y})^2}} \quad (3)$$

In the formula, R is the correlation coefficient of x and y, n is the number of years of study time, x_i is the VIs in the i-th year, and y_i is the average annual the SFR and the SM values in the i-th year.

2.6. Assessing the effect of long-term correlation

The Hurst index can quantitatively describe the degree of dependence of a sequence over a long period of time; so, it can be used to judge whether the future change in the sequence will be continuous.

Then, the degree of continuity is described by classifying the numerical values. The assessment methods of the Hurst index mainly include the absolute value method, aggregate variance method, rescaled range (R/S) analysis method, periodogram method, Whittle method, residual variance method, and wavelet analysis method. In this study, the aggregate variance method was used to assess the Hurst exponent of the correlation coefficient. The principle is to divide the given time series (X_i, i = 1, 2, …, N) into [N/m] subintervals of equal length (Tomsett and Toumi, 2001). We separately calculated this in each subinterval to obtain the average of each interval:

$$X_m(k) = \frac{1}{m} \sum_{i=(k-1)m+1}^{k_m} x_i, k = 1, 2…, [N/m] \quad (4)$$

Then, the sample variance of its mean was calculated:

$$V_{ar}X_m = \frac{1}{N/m} \sum_{k=1}^{N/m} \left[X_m(k)-\overline{X}\right]^2 \quad (5)$$

If the sequence has long-term dependence, Var Xm ~ mα is established. On the logarithmic graph of (m/VarXm), the slope is α through linear function fitting; so, H = (α/2) + 1. The slope interval can be divided into the following three situations (Montanari et al., 1999): (1) If 0 ≤ H ≤ 0.5, the changes in the correlation time series of the vegetation indicators (VIs) with SFR and SM exhibit reverse persistence. When the H value tends to 0, the anti-sustainability becomes stronger. (2) If H = 0.5, the correlation time series has a weak correlation, and it can be inferred that the future change trend of the factor limitation is not related to the past changes. (3) If 0. 5 ≤ H ≤ 1, the change in the time series exhibits positive continuity, that is, it can be inferred that the future change trend of the factor is consistent with the past changes. When H approaches 1, the continuity is stronger.

2.7. Univariate linear regression analysis

In this study, unitary regression trend analysis was used pixel-by-pixel to analyze the spatial and temporal evolutions of the correlations between the VIs and the environmental factors in the global karst region from 2000 to 2014. The calculated slope reflects the trend of the evolution of each indicator (Gong et al., 2021; Zhang et al., 2021c). A slope of greater than 0 indicates that the pixel exhibited an increasing trend during 2000–2014, and vice versa. The magnitude of the slope reflects the sharpness of the ascent and descent in the pixel. The greater the magnitude of the absolute value of the slope, the more severe the change. The formula is as follows:

$$\theta = \frac{n \times \sum_{i=1}^{n}(i \times A_i) - \left(\sum_{i=1}^{n}i\right)\left(\sum_{i=1}^{n}A_i\right)}{n \times \sum_{i=1}^{n}i^2 - \left(\sum_{i=1}^{n}i\right)^2} \quad (6)$$

where θ is the evolution trend, i is the difference index value, n is the number of changes, and A_i is the correlation between the different index under the ith change.

2.8. Statistical analysis of static data indicators

By using a moving window composed of 11 × 11 grid cells (5.5° × 5.5°) to calculate the local correlation (Carvalhais et al., 2014) and to simulate the regression trend, the correlation and changes between the VR and TH and the SFR and SM were evaluated for each grid cell of the global data. This method can reveal the local importance of the SFR and SM at the pixel scale and can be used to obtain a more accurate global estimate of the regional change between them. Through Pearson correlation analysis and univariate linear regression analysis, the relationship between the vegetation properties and soil can be determined. Such analysis can further clarify the relative importance of

the SFR and SM in determining the global spatial pattern of vegetation growth.

3. Results

3.1. Dual limiting effects of the SFR and SM on vegetation in global karst regions

From 2000 to 2014, the global soil environment continued to fluctuate, which was affected by global warming and other climatic conditions. The key factor (SM) in the global karst areas exhibited a downward trend, even though it was higher in the karst areas than in the non-karst areas. However, the NPP in the karst areas around the world continued to increase (Fig. S1), and the vegetation indicators were lower than those in non-karst areas (Fig. S2). We conclude that this may be due to the increase in the SFR, which created favorable soil conditions for the growth and productivity of vegetation.

Fig. 1 shows the spatial correlations between the NPP and the SFR and SM ($R_{Npp-SFR}$, R_{Npp-SM}). In high-latitude and low-latitude cold regions (such as the Qinghai-Tibetan Plateau), the SFR and SM were negatively correlated with the NPP, that is, the higher SFR and SM values corresponded to weaker VG (-0.03, -0.1). In the low- and mid-latitude regions, the correlation was the opposite, especially in a grassland climate with less precipitation. The increase in the SFR and SM drove the increase in the NPP to a greater extent (0.21, 0.41). These results show that if we used different NPP data instead of the NPP data from the MODIS datasets, a similar pattern would also be found (Fig. S3). Thus, all these demonstrate that our results are reliable. We concluded that the positively correlated variables were the factors limiting the ecosystem productivity because increasing these factors is beneficial in most situations. Moreover, when the NPP was limited by the

SFR, this state presented an increasing trend and maintained a strong continuity. This was also true for the SM. It should be noted that the current non-limitation areas may become limitation areas due to the effects of the SFR and SM over time (Fig. 1C and D). This indicates that the limitation of the NPP by the SFR and SM may become more obvious in the future, which constrains the NPP in karst areas and affects the VG.

Fig. 2B shows that the correlation between the SFR-NPP correlation coefficient ($R_{Npp-SFR}$) and the SFR-NPP correlation coefficient (R_{Npp-SM}) was positive ($R = 0.456$, $P < 0.05$), which indicates that in most regions, the NPP was subject to the common limitations of the SM and SFR. When the SFR lost its limiting effect on the VG, the effect of the surface SM also disappeared. More than 70% of the global climate zones clearly exhibited the dual limitations of the SM and SFR, and the climate zones constrained by the SFR alone accounted for 88.46% of the total (Fig. 2A), which shows that except for extreme climate zones, the vegetation in the global karst areas was limited by the SFR.

Compared with the NPP, the latitude of the positive correlations between the SFR and SM and the NDVI ($R_{NDVI-SFR}$, $R_{NDVI-SM}$) is shifted downward by 20°–30°. However, the number of global positive correlations was also greater than the number of negative correlations, and this trend will continue to grow in the future. This different pattern is interpreted as representing a lesser reliance of the degree and scope of the NDVI on the SFR and a greater reliance on the SM processing (Fig. S4), especially in the hinterlands of Eurasia and South America (Brazil).

At almost all latitudes, we found positive and negative correlations between the SFR and SM and the TH and VR (R_{TH-SFR}, R_{TH-SM}, R_{VR-SFR}, and R_{VR-SM}), and these ranges were intertwined. In the Northern Hemisphere, the R_{TH-SFR} was more positive than the R_{TH-SM} (Fig. S5). However, near the equator, the increase in the SFR in most areas reduced the TH, which may be because the impact of the SM was even
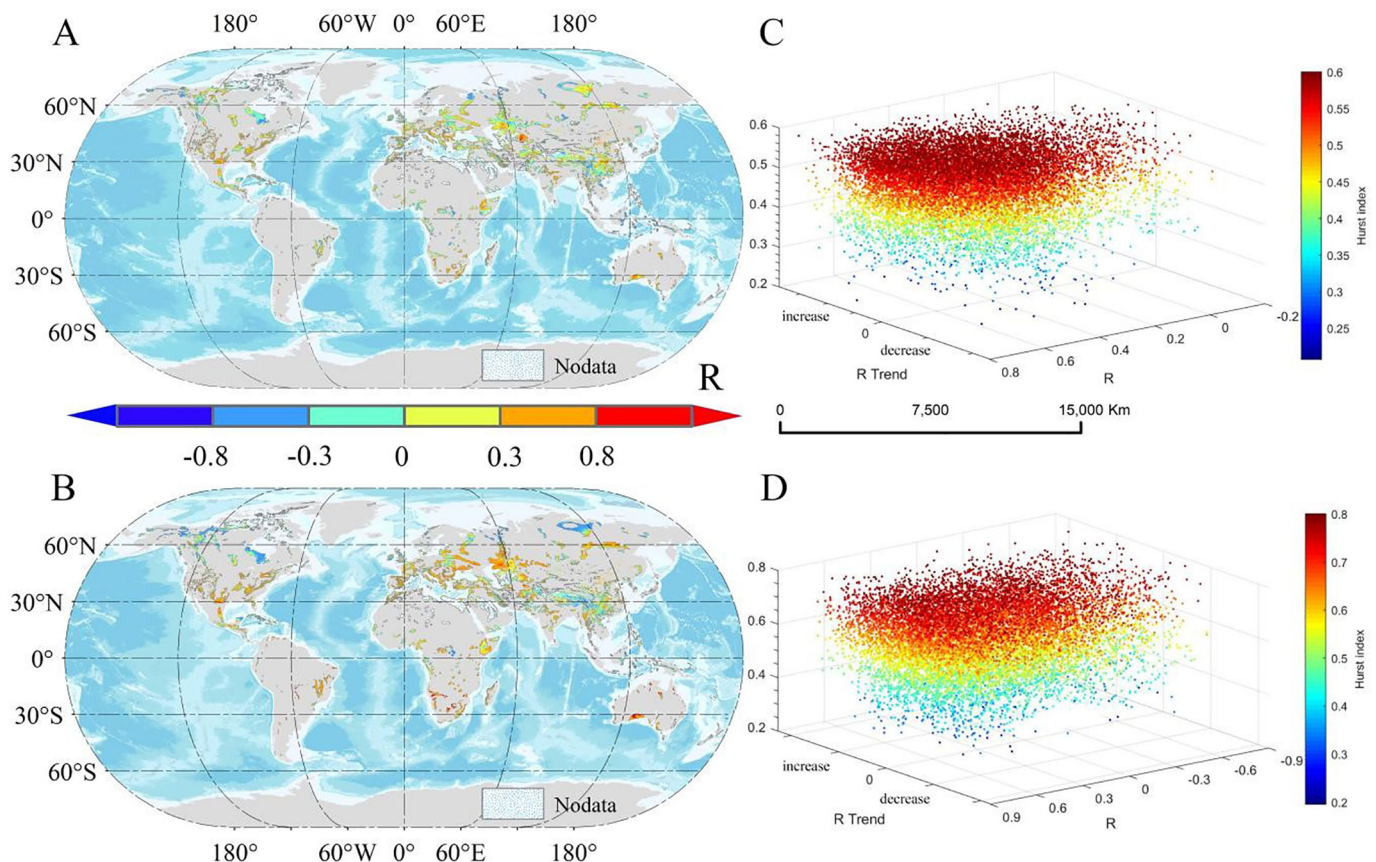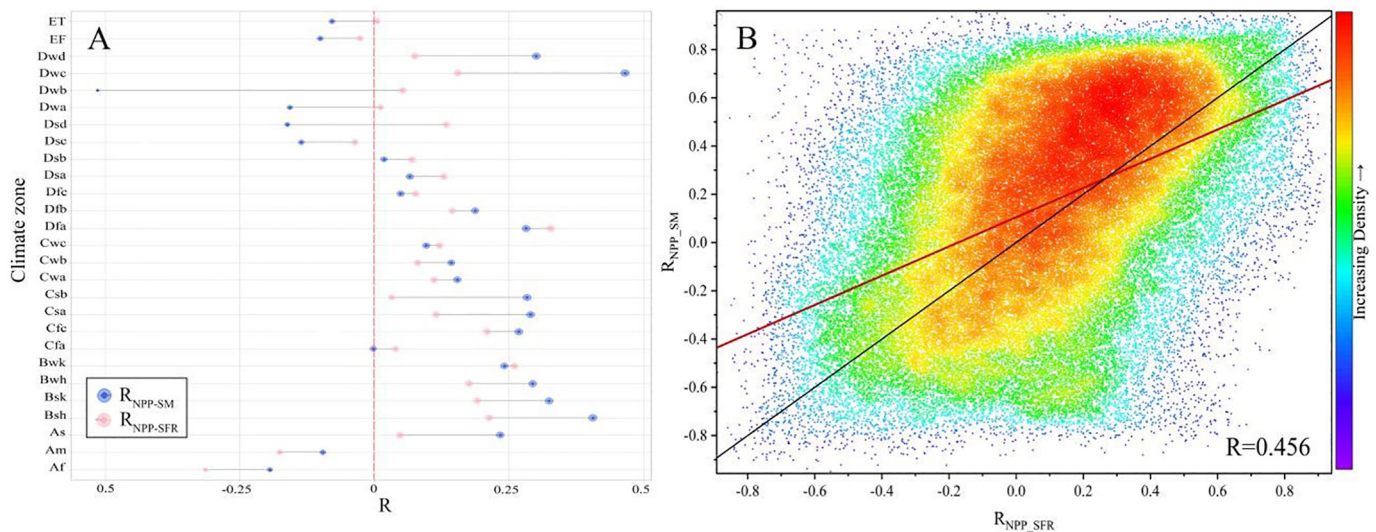

Fig. 1. The $R_{NPP-SFR}$ (A) and R_{NPP-SM} (B). And the relationship between their trend changes, Huster index and correlation coefficient (C, D).

Fig. 2. The average of $R_{NPP-SFR}$ and R_{NPP-SM} in Karst on the Köppen climate zone (A). And the correlation between the $R_{NPP-SFR}$ and R_{NPP-SM} (B). (Af) tropical rainforest climate; (Am) tropical monsoon climate; (Aw) tropical dry and wet season climate; (Bwh, Bwk) desert climate; (Bsh, Bsk) semi-arid climate; (Cfa, Cwa) subtropical humid climate; (Cfb, Cwb, Cwc, Cfc) maritime climate; (Csa, Csb) Mediterranean climate; (Dsa Dfa, Dwa, Dsb, Dfb, Dwb) continental humid climate; (Dfc, Dwc, Dfd, Dwd, Dsc, Dsd) subpolar climate; (ET, EF) polar climate.

stronger. In terms of the VR, although the numbers of pixels with positive and negative R_{VR-SFR} and R_{VR-SM} were roughly the same, the intensity of the R_{VR-SM} was much higher than that of the R_{VR-SFR}. In addition, near the Great Australian Bay Desert, the increase in the SM may have suppressed the VR. This demonstrates that the SM has a deeper influence on the VR, regardless of the overall average or spatial pixel points (Fig. S3).

3.2. Dynamic limitation zone of vegetation in karst areas

According to the changes in the SM and SFR and their correlations with the various vegetation indicators, the dynamic limitation zones of the NPP, NDVI, VR, and TH (685.19 km^2, 615.13 km^2, 701.97 km^2, and 382.06 km^2, respectively) were determined (Table 1). Using the above method, we estimated that 50% of the VR of the karst areas in the world were the most strongly affected by the limiting factors, and even the smallest limitation zone of the TH accounted for 26% of the world's karst areas. This further supports the conclusion that the changes in the SFR and SM were related to the growth and development of the vegetation in karst areas to a greater extent, and the differences in the responses of the different vegetation characteristics to them were also obvious.

The changes in the SFR and SM mainly exhibited a superimposed effect on the NPP, with an area of about 311.08 km^2 (Fig. 3). However, the remaining indicators mainly had a single SM-limitation zone during the study period (Figs. S5–7). We analyzed the changes in the NPP and NDVI in the dynamic limitation zone from 2000 to 2014 and found that the zone affected by the SFR expanded, while that affected by the SM slowly contracted (Fig. S6). This occurred because the areas with an SM drying trend expanded, and the SFR continued to decline in the dynamic limitation zone, even when the overall trend of the SFR was slowly

increasing due to the impact of global warming. The vegetation in the karst areas cannot eliminate the negative effects of both the SM and SFR at the same time; so, there was still a large area of vegetation that was limited in terms of its growth and development.

The results were further linked with specific spatial regions, and 10 countries with the largest regional karst distribution in the world were selected (Figs. 3; S7–9). These countries were located in the dynamic limitation zone of the VIs. Except for the NDVI, Russia, which accounted for the largest proportion of the karst areas, had the largest dynamic limitation zone. Although India did not have the smallest karst area of the 10 countries, the impact of the SM and SFR on the VG was very small, and the largest zone only occupied 6.05 km^2 (VR). The different VIs of Kazakhstan (KAZ) had very different responses to the decreases in the SFR and SM. The VR of KAZ was the most sensitive to the changes in soil and water, and it occupied an area greater than that in Russia, but only 7.66% of the country's TH in the karst areas became shorter as the SFR and SM decreased. Moreover, the SFR-limited zones in all of the countries also had SM-limited zones, the proportions of which were not low, that is, the dynamic changes in the SM during 2000–2014 exacerbated the limitation of the SFR on VG. More importantly, the range of vegetation limited by the SM in these countries was much larger than that limited by the SFR, except in Brazil. This may be because the SFR and SM in Brazil mainly exhibited trends of decline and growth, respectively, during the study period, and the area with a decrease in the SM coincided with the area in which the SFR decreased.

3.3. Ecological thresholds in different ecological regions

The vegetation distribution pattern is the result of the coupling of multiple factors (Marrs and Due, 2000; Michael and Thomas, 2001;

Table 1
The dynamic SFR-limited and SM-limited areas (10^4 km^2) for vegetation indicators.

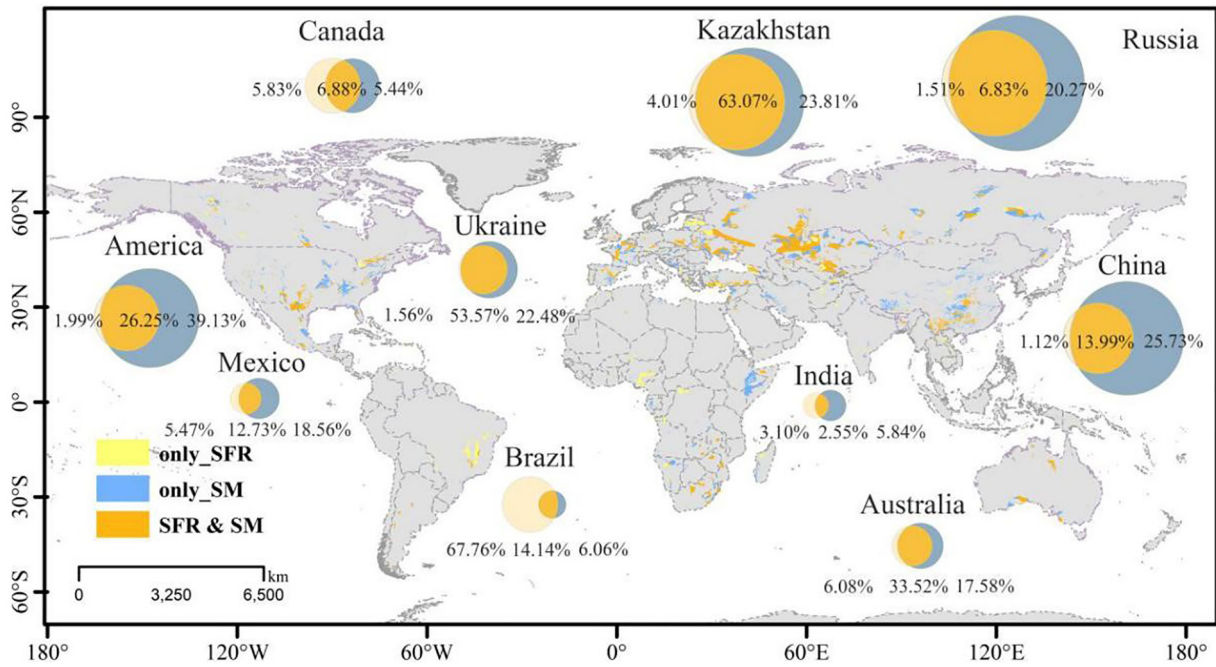|	only_SFR_AREA	only_SM_AREA	SFR&SM_AREA	Limitation AREA	Account for
NPP	93.91	280.2	311.08	685.19	47.99%
NDVI	121.13	311.06	182.94	615.13	43.09%
VR	171.25	409.53	121.19	701.97	49.17%
TH	88.48	232.59	60.98	382.06	26.76%
Total					1427.67

Fig. 3. The dynamic limitation zone of the SFR and the SM for NPP in karst areas. 10 countries with the highest karst distribution were selected to analyze their proportions subject to limitation of the SFR and SM.

Svenning et al., 2004). Therefore, we divided the world into different ecological regions for more specific and detailed analysis and controlled the climate variables in these regions. As can be seen from Figs. S10–12, the SFR and SM increases were observed to affect the NPP, NDVI, VG, and TH in the different ecological regions. The area between the upper and lower solid lines in the figure was the control area of each indicator, which represents the maximum possible fluctuation range of each indicator under different SFR and SM conditions. The points outside the control area represent abnormally good or poor values of each indicator. The coordinate of the center point of the area between the two shaded areas in the figure was regarded as the sensitive point of the indicator's change, which is the threshold of the transition between the different vegetation growth states in the karst areas.

The results show that the thresholds of the SRF and SM affected a series of vegetation states in the different ecological regions, but the intensity and breadth of this influence were different. Among all of the ecological regions, only the NPP, NDVI, VR, and TH were limited by the SFR and SM in Taiga. When the SFR increased to 25.163 t km^{-2} yr^{-1},

the inflection point of the NPP, NDVI, and TH appeared. At this time, the NPP jumped from 320 g m^{-2} to 491 g m^{-2}. The percentage increase reached 53.44%. When the SFR increased to 0.318 m^3 m^{-3}, the vegetation status also increased sharply, indicating that the vegetation in this region was heavily dependent on soil formation through weathering, and the SM may be the main mechanism of water resource supply. The opposite situation occurred in the mangrove areas. If and only if the NDVI increased from 0.44 to 0.70, the SFR threshold was 25.044 t km^{-2} yr^{-1}, with 94% confidence. The increase or decrease in the SM did not affect the growth and development of the mangroves. Flooded grasslands and savannas and temperate broadleaf and mixed forests exhibited similar situations regarding the SM limitation. The tropical and subtropical dry broadleaf forests, tropical and subtropical coniferous forests, deserts, and xeric shrublands were not affected by the SFR.

In general, when the SFR and SM were 25.028–25.631 t km^{-2} yr^{-1} and 0.221–0.339 m^3 m^{-3}, respectively (Fig. 4), different VIs would exhibit step-like increases. The VR was the least sensitive to the changes in the SFR and SM. The VR had the highest requirements under SM
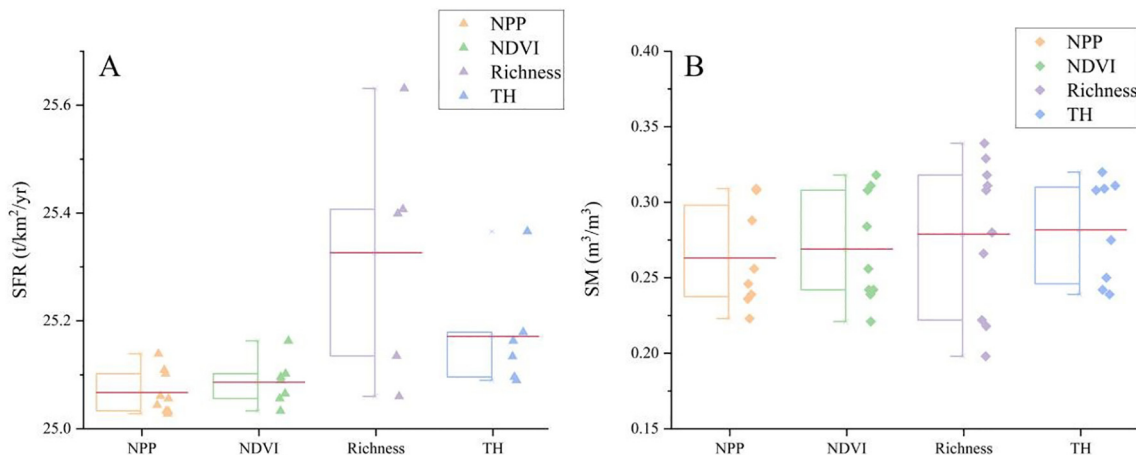

Fig. 4. Threshold statistics of global karst the SFR (A) and SM (B) for different vegetation indicators.

and SFR conditions, and the average threshold values of the VR were also the largest among those of the other VIs. We believe that vegetation will grow better only when the SFR and SM are greater than the threshold corresponding to the characteristics of each plant community.

3.4. Current patterns of the SFR and SM limitations on karst vegetation

Herein, we delineated the area below the threshold point from 2000 to 2014 as the static vegetation limitation zone. As shown in Fig. S13, most of the karst areas in the world were affected by the SFR and SM, which made them high-risk areas for vegetation degradation. This made these areas unable to maintain the necessary ecological conditions for biological survival, which would have a negative impact on human well-being in the global karst areas.

The effects of the SFR and SM on the different vegetation characteristics exhibited spatial differences. Under different VIs, each SM-limited zone was relatively consistent. For the SFR, the opposite was true (Fig. 5). The SFR limited 47.73% of the vegetation in the global karst areas, and the SM-limited zone accounted for 43.44% (Fig. S13). As can be seen from Table S2, it can be clearly found that the area where the VR was inhibited by the SFR during the study period was the widest (up to 681.375 km^2). This area was much larger than that of the SM (558.86 km^2). The results show that the SFR in karst areas mainly limited the growth of the NPP above 30°N, but the limited performance of the NDVI was observed in only 25.02% of the area because the NDVI was mostly limited by the SFR and was also suppressed by the SM. It was confirmed that the dual limiting effect of the SFR and the SM was mainly concentrated in southwestern China and Central Asia. The limitation of the TH was similar to that of the NDVI, but it was mainly concentrated in Central Asia and eastern Russia. The VR had another limitation distribution. For example, the VG on the Qinghai-Tibetan Plateau was mainly controlled by the SM instead of the SFR. The VG in the Southern Hemisphere was almost only limited by the low SFR. This phenomenon once again illustrates the limitation of the VG by the SFR. Only when the SFR reaches a higher level will the soil accumulate to a certain thickness and produce enough nutrients and microorganisms for the growth and development of more types of plants.

The vegetation in Asian karst areas may be more dangerous than that on other continents (Fig. 5). Both the SFR and SM limited a large amount of vegetation in Asia, especially in terms of the NDVI and TH and mainly on the Qinghai-Tibetan Plateau. In the Eurasian karst areas, the area where the NDVI was limited by the SFR was the smallest (Fig. 5A). Oceania has a smaller karst area; so, the local karst vegetation was less disturbed by the SFR and SM compared to that on other continents. However, it is undeniable that except for the NPP in the northern part of the site, which was almost unlimited by the two factors, the

limited zones of the other VIs covered almost the entire karst areas of Oceania. The main reason for this was that the larger area of the SM was below the threshold. For the ecological region, it is obvious that more vegetation types were affected by the SM than by the SFR. Unlike the distribution of vegetation, which was affected by the SFR, the area only limited by the SM in the desert grassland.

4. Discussion

4.1. Comparison with related studies

We compared the SFR calculated in this study with other scholars' results to further confirm the reliability of our results. Most previous studies of the SFR in karst areas focused on China and parts of China, which are rich in karst environment resources. We believe that the average SFR on the national scale should be within the results range of other scholars. Therefore, we compared the Chinese-scale SFR calculated in this study with the results of different scholars. In this study, the SFR of the karst areas in China was calculated to be 25.76 t km^{-2} yr^{-1}, while Li et al. (2020) reported that the average SFR in China from 1983 to 2015 was 18.59 t km^{-2} yr^{-1}, which is slightly smaller than the result obtained in this study. This may be caused by ignoring the influence of the carbonate and clastic rock interbedded assemblage (CA) area and the differences in the lengths of the study periods. Li et al. (2006) calculated the SFR of Guizhou Province to be 6.75–103.46 t km^{-2} yr^{-1} in 2006. Cao et al. (2008) found that the SFR in Southwest China was 4–120 t km^{-2} yr^{-1}. Li et al. (2017) calculated the allowable loss in southern China to be in the SFR range of 20 < SFR ≤ 100 t km^{-2} yr^{-1}. The results of this study are all within the range of variation defined by these different research results; so, we believe that the calculation of the SFR in this study is reliable.

Deng et al. (2020a, 2020b) found that due to the influence of the thickness of the soil layer, the SM in China's karst areas was higher than that in its non-karst areas. This was also observed when the research was extended to the global scale. In addition, plant physiological phenology (end-of-season photosynthesis) was more sensitive to environmental changes. Several scholars have conducted research on the limitation of the SM on vegetation photosynthesis (Zhang et al., 2020). They found that the SM and vegetation photosynthesis also had a positive spatial correlation, which further demonstrates that the SM had confinement effects on the VG in space.

4.2. Differences in the thresholds in different ecological regions

The SRF and SM were found to affect a series of vegetation characteristics (Fig. 4) in different ecological regions. When the areas limited by
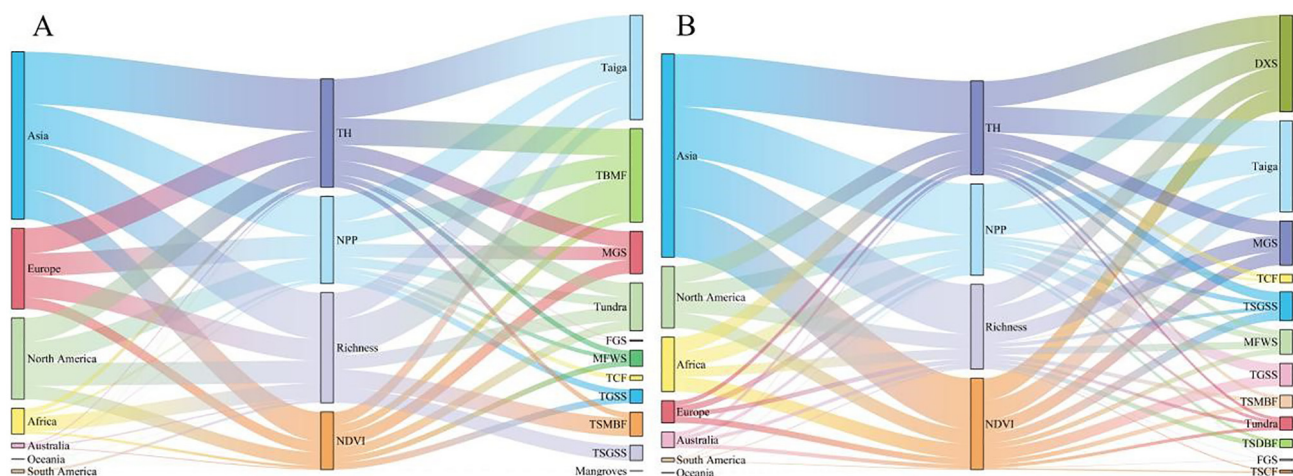

Fig. 5. The SFR-limited and SM-limited diversion for vegetation indicators from different continents or ecological regions.

the SFR and SM are excluded, the relationship between the climate and vegetation is further strengthened (Fig. S14). However, the intensity and breadth of this impact were different due to the different climate and vegetation habits (Wang et al., 2020a).

In tropical and subtropical moisture broadleaf forests, the vegetation is mainly controlled by the water conditions (Yan et al., 2013). Therefore, changes in the SFR do not affect it. The growth of Hardwood shrub and hardwood canopy or emergent hardwood shrub requires favorable environmental conditions. They need thick soils to survive (Zhang and Zang, 2007). This makes it possible to meet the normal living conditions of these plants only when the SFR is greater than 25.631 t km^{-2} yr^{-1}, thereby enriching the species richness of the tall vegetation in this ecological region and increasing its average TH. In terms of the SM conditions, O'Connell et al. (2018) investigated the humid tropical forests of Puerto Rico and found that these humid tropical forests respond positively to decreased SM. As the soil gradually dried (SM < 0.28 m^3 m^{-3}), the litter of the vegetation gradually increased, and the biomass and TH began to decrease (Giardina et al., 2018) because that moisture was not sufficient to be transported to the higher canopy. However, the soil desiccation affected the death of the vegetation through hydrodynamics rather than carbon starvation of tropical rain forest vegetation (Guo et al., 2018). Thus, for this zone, the NPP had no corresponding ecological threshold. Fig. S12 also shows that both the SFR and SM limited the abundance of vegetation before causing the decline in the TH. This also demonstrates that compared with other plants, tall trees require more water and a greater soil thickness to support their growth and development. Moreover, this also resulted in the 31.19 × 10^4 km^2 of karst tropical rainforest facing degradation into a savanna under the limitation of the SM, and the low SFR expanded such high-risk areas by 13.90% (Table S2).

The savanna was generally distributed in Africa, Australia, and North and South America with high temperatures throughout the year and distinct dry and wet seasons. It is a thermal ecosystem with symbiosis of perennial drought-tolerant herbs, shrubs, and isolated trees (Harris, 1980; Walter, 1994). The VG in this ecological region is mainly limited by water (Walker et al., 1981); so, the VIs had a positive response to the SM (Sankaran et al., 2005). When the SM gradually reached the threshold range (0.239–0.339 m^3 m^{-3}), the NPP, NDVI, VR, and TH of the savanna increased. We speculated that under these conditions, the grass and trees were in stable symbiosis. In particular, if the SM exceeds 0.339 m^3 m^{-3}, tall trees may appear in this area. In addition, if the SM decreases to <0.198 m^3 m^{-3}, the ecosystem may be severely damaged and may degenerate into tropical grasslands. Tropical and subtropical dry broadleaf forests are ecological regions composed of hard-leaved broadleaf forest vegetation in dry and hot valleys. Unlike Mediterranean forests, the climate here is warm and hot and dry and cold at the same time. In addition, the vegetation has the ability to adapt to droughts and heat. The main types of natural vegetation are Woodfordia fruticosa (L.) Kurz., Heteropogoneontortus, savanna shrubs, dry grass, and succulent prickly shrubs such as cacti on the stony surfaces. Therefore, this vegetation has a strong ability to survive and is widely distributed in limestone mountains with shallow soil layers (Jiang, 1980; Jin and Qu, 1981). Moreover, the change point further demonstrates that the SFR did not have a severe impact in this zone, that is, there was no ecological threshold for the SFR. However, the continuous increase in the SM inhibited the normal growth of this vegetation, causing the NPP to drop below 0.223 m^3 m^{-3}. In addition, when the SM further increased to 0.339 m^3 m^{-3}, the productivity of some moisture-loving vines increased to enrich their species.

With the latitude shifting to the north, the temperate broadleaf and mixed forests were luxuriant in summer and sparse in winter, but the SM did not change simultaneously with the phenology. Jin et al. (2017) studied the response of the water use efficiency (WUE) to the flux-based photosynthetic onset and found that the WUE in spring had a significant positive response to the advanced photosynthesis in this zone, which caused the SM to decrease and led to summer water

stress (Leuzinger et al., 2005; Kljun et al., 2006). In autumn and winter, the climate was cold with little rain, and the vegetation evapotranspiration was low. Although the SM was low, the vegetation absorption was weak, and the change in the SM was not significant. In contrast, in spring and summer, the temperature increased significantly, the vegetation activity was vigorous, and the evaporation of the forest soil and vegetation was strong, which led to serious loss of SM. This phenomenon allowed the vegetation to grow rapidly, even under the extreme SM deficiency (Meehl and Tebaldi, 2004). In addition to climate factors, the increase in the SFR had a huge impact on the temperate broadleaf and mixed forests. One reason for this was that soil microorganisms affected the plant communities (You et al., 2020; van der Putten et al., 2013) through the availability of soil nutrients. In addition, the increase in the SFR expanded their breeding and living space. Another reason for this was that China, Europe, and North America, which have the best conditions for the growth of temperate broad-leaved forests, have become the largest acid deposition areas (Wang et al., 2014), which affects the normal growth and development of vegetation. The decrease in the SFR in forests reduces the soil organic matter content (Mo et al., 2003), which in turn causes a decrease in the CEC (the number of moles of exchangeable cations electrostatically adsorbed per unit mass of soil) and the soil acid buffer capacity (Fang et al., 2017). Therefore, when the SFR was greater than 25.407 t km^{-2} yr^{-1}, the growth and development of the vegetation in this zone could be satisfied. It should be noted that the SFR values below the global threshold were mostly distributed in the three major acid rain regions of the world, which may lead to further forest degradation in the future (Fig. S13).

Taiga was the only ecological region where the different VIs had thresholds for both the SFR and SM, that is, the SFR and SM were both important environmental factors and influenced the vegetation changes in Taiga. This zone is mainly composed of cold-resistant coniferous trees, and they are often pure forests composed of a single species. The main tree species are shallow-rooted vegetation (e.g., spruce, fir, and larch) and are susceptible to environmental factors. Among them, the soil fertility is an important factor influencing the VG, and the SM plays an important positive role in the soil organic carbon content in Taiga (Sewell et al., 2020). When the SM was greater than 0.322 m^3 m^{-3}, it may have offset the loss of coniferous forest due to warming and wildfires (Petrie et al., 2016; D'Orangeville et al., 2018). In addition, we also believe that areas with consistently high SFRs can accumulate thicker soil layers on a long-time scale, and they have a stronger ability to resist soil erosion. In addition, Liu and Yang (2014) reported that wildfires consumed the surface soil layer. Therefore, only a higher SFR can reduce the soil loss rate, which will help the seeds to germinate quickly and achieve effective vegetation restoration.

4.3. Uncertainty and future perspectives

The results of and assumptions made in this study are uncertain. In terms of the SFR calculation, the influence of the carbonate and CA area was ignored, even though it accounts for a small area. Thus, in order to more accurately quantify the magnitude and distribution of the SFR, it is necessary to further unify the classification of the karst areas and confirm the distribution areas of the different lithological combinations in order to improve the reference significance of the results.

In terms of the SM, in this study, only the surface SM (0–7 cm) was evaluated. However, the reachable depths of the roots of different vegetation are different, and the deeper SM may also affect the regularity and maintenance of the normal growth and development of vegetation. This needs to be explored further. In future research, the impact of the SM at different soil depths on vegetation should be studied to enable more accurate judgment of the changes in the ecological threshold of the SM in the vertical direction.

Finally, in this study, different ecological regions were used to control the main environmental variables, such as the temperature and

precipitation, as much as possible, but the soil bulk density, soil microbes, and the thickness of the soil surface organic matter layer are also different in the different zones. They all create living conditions for vegetation growth and supply nutrients, and they lead to the different morphological characteristics of the vegetation in karst areas. Consequently, the results obtained in this study lack comprehensive control over variables. We will devote more attention to the effects of different factors in related research in the future.

5. Conclusions

Based on high-precision ecological, hydrological and meteorological spatial datasets, using trend analysis, correlation analysis, and change point analysis methods, we found vegetation changes in karst areas were obviously controlled by SFR and SM. In addition, we established further a spatial map ($0.125° \times 0.125°$) of the global karst ecosystem with a static/dynamic limitation zone based on the SFR and SM thresholds. The conclusions are the following:

(1) the limitation of the NPP by the SFR and SM may become more obvious in the future, which constrains the NPP in karst areas and affects the VG. Moreover, except for extreme climate zones, the vegetation in the global karst areas was limited by the SFR.

(2) The dynamic limitation zones of NPP, NDVI, VR and TH covered an area of 685.19 km^2, 615.13 km^2, 701.97 km^2, and 382.06 km^2, respectively. We estimated that 50% of the VR of the karst areas in the world were the most strongly affected by the limiting factors, and even the smallest limitation zone of the TH accounted for 26% of the world's karst areas.

(3) In 10 countries with the largest karst regional distribution, the dynamic changes in the SM during 2000–2014 exacerbated the limitation of the SFR on VG. More importantly, the range of vegetation limited by the SM in these countries was much larger than that limited by the SFR, except in Brazil.

(4) When the SFR and SM were 25.028–25.631 t km^{-2} yr^{-1} and 0.221–0.339 m^3 m^{-3}, respectively, different VIs would exhibit step-like increases. In addition, the SFR limited 47.73% of the vegetation in the global karst areas, and the SM-limited zone accounted for 43.44%.

(5) the 31.19×104 km^2 of karst tropical rainforest facing degradation into a savanna under the limitation of the SM, and the low SFR expanded such high-risk areas by 13.90%.

Data availability

The authors declare that the source data supporting the findings of this study are provided within the paper.

CRediT authorship contribution statement

Sirui Zhang: Conceptualization, Formal analysis, Writing – original draft. **Xiaoyong Bai:** Conceptualization, Supervision, Resources. **Cuiwei Zhao:** Validation, Project administration. **Qiu Tan:** Validation, Project administration. **Guangjie Luo:** Validation, Project administration. **Yue Cao:** Validation, Formal analysis. **Yuanhong Deng:** Validation, Formal analysis. **Qin Li:** Validation, Formal analysis. **Chaojun Li:** Data curation, Writing – review & editing. **Luhua Wu:** Data curation, Writing – review & editing. **Jinfeng Wang:** Data curation, Writing – review & editing. **Fei Chen:** Data curation, Writing – review & editing. **Huipeng Xi:** Visualization. **Chen Ran:** Visualization. **Min Liu:** Visualization.

Declaration of competing interest

The authors declare that they have no known competing financial interests or personal relationships that could have appeared to influence the work reported in this paper.

Appendix A. Supplementary data

Supplementary data to this article can be found online at https://doi.org/10.1016/j.scitotenv.2021.151209.

References

Amundson, R., 2021. Factors of soil formation in the 21st century. Geoderma 114960, 0016–7061. https://doi.org/10.1016/j.geoderma.2021.114960.

Bai, Y.Q., Yang, Y.P., Jiang, H., 2019. Intercomparison of AVHRR GIMMS3g, Terra MODIS, and SPOT-VGT NDVI products over the mongolian plateau. Remote Sens. 11, 2030. https://doi.org/10.3390/rs11172030.

Cao, J.H., Jiang, Z.C., Yang, D.S., Pei, J.Z., Yang, H., Luo, W.Q., 2008. Soil Loss Tolerance and Prevention and Measurement of Karst Area in Southwest China (in Chinese). Soil and Water Conservation in China. 12, pp. 40–45.

Cao, J.H., Jiang, Z.H., Yuan, D.X., Xia, R.Y., Zhang, C., 2017. The progress in the study of the karst dynamic system and global changes in the past 30 years (in Chinese). Geol. China 44, 874–900.

Carvalhais, N., Forkel, M., Khomik, M., Bellarby, J., Jung, M., Migliavacca, M., Mu, M.Q., Saatchi, S., Santoro, M., Thurner, M., Weber, U., Ahrens, B., Beer, C., Cescatti, A., Randerson, J.T., Reichstein, M., 2014. Global covariation of carbon turnover times with climate in terrestrial ecosystems. Nature 514, 213–217. https://doi.org/10.1038/nature13731.

Cowling, R.M., Richardson, D.M., Pierce, S.M., 1997. Cambridge Univ Press, New York.

D'Orangeville, L., Houle, D., Duchesne, L., Phillips, R.P., Bergeron, Y., Kneeshaw, D., 2018. Beneficial effects of climate warming on boreal tree growth may be transitory. Nat. Commun. 9, 3213. https://doi.org/10.1038/s41467-018-05705-4.

Deng, Y.H., Wang, S.J., Bai, X.Y., Luo, G.J., Wu, L.H., Cao, Y., Li, H.W., Li, C.J., Yang, Y.J., Hu, Z.Y., Tian, S.Q., 2020. Variation trend of global soil moisture and its cause analysis. Ecol. Indic. 110, 105939. https://doi.org/10.1016/j.ecolind.2019.105939.

Deng, Y.H., Wang, S.J., Bai, X.Y., Luo, G.J., Wu, L.H., Chen, F., Wang, J.F., Li, C.J., Yang, Y.J., Hu, Z.Y., Tian, S.Q., Lu, Q., 2020. Vegetation greening intensified soil drying in some semi-arid and arid areas of the world. Agric. For. Meteorol. 292–293, 108103. https://doi.org/10.1016/j.agrformet.2020.108103.

Dolan, K.A., Hurtt, G.C., Flanagan, S.A., Fisk, J.P., Sahajpal, R., Huang, C.Q., Page, Y.L., Dubayah, R., Masek, J.G., 2017. Disturbance distance: quantifying forests' vulnerability to disturbance under current and future conditions. Environ. Res. Lett. 12 (11). https://doi.org/10.1088/1748-9326/aa8ea9.

Fang, K., Kou, D., Wang, G.Q., Chen, L.Y., Ding, J.Z., Li, F., Yang, G.B., Qin, S.Q., Liu, L., Zhang, Q.W., Yang, Y.H., 2017. Decreased soil cation exchange capacity across northern China's grasslands over the last three decades. J. Geophys. ResBiogeosci. 122, 3088–3097. https://doi.org/10.1002/2017JG003968.

Finlayson, B.L., Mcmahon, T.A., 2007]. Updated world map of the Köppen-Geiger climate classification. [dataset]Hydrol. Earth Syst. Sc. 11, 259–263.

Giardina, F., Konings, A.G., Kennedy, D., Alemohammad, S.H., Oliveira, R.S., Uriarte, M., Gentine, P., 2018. Tall Amazonian forests are less sensitive to precipitation variability. Nature Geosci. 11, 405–409. https://doi.org/10.1038/s41561-018-0133-5.

Gombert, P., 2002. Role of karstic dissolution in global carbon cycle. Glob. Planet. Chang. 33, 177–184. https://doi.org/10.1016/S0921-8181(02)00069-3.

Gong, S.H., Wang, S.J., Bai, X.Y., Luo, G.J., Wu, L.H., Chen, F., Qian, Q.H., Xiao, J.Y., Zeng, C., 2021. Response of the weathering carbon sink in terrestrial rocks to climate variables and ecological restoration in China. Sci. Total Environ. 750 (1), 141525. https://doi.org/10.1016/j.scitotenv.2020.141525.

Gonsamo, A., Chen, J.M., Lombardozzi, D., 2016. Global vegetation productivity response to climatic oscillations during the satellite era. Glob. Change Biol. 22, 3414–3426. https://doi.org/10.1111/gcb.13258.

Guo, Y.L., Xiang, W.S., Wang, B., Li, D.X., Mallik, A.U., Chen, H.Y.H., Huang, F., Ding, T., Wen, S.J., Lu, S.H., Li, X.K., 2018. Partitioning beta diversity in a tropical karst seasonal rainforest in southern China. Sci. Rep. 8, 17408. https://doi.org/10.1038/s41598-018-35410-7.

Harris, D.R., 1980. Human Ecology in Savanna Environments. Academic Press, London.

Hartmann, J., Lauerwald, R., Moosdorf, N., 2019]. GLORICH - Global river chemistry database. [dataset]Pangaea 10, 23–27. https://doi.org/10.1594/PANGAEA.902360.

Idso, S.B., Kimball, B.A., 1993. Tree growth in carbon-dioxide enriched air and its implications for global carbon cycling and maximum levels of atmospheric CO2. Glob. Biogeochem. Cycl 7, 537–555. https://doi.org/10.1029/93GB01164.

Jiang, H.J., 1980. Distribution features and zonal regularity of vegetation in Yunnan (in Chinese). Acta Bot. Yunnanica 02, 142–151.

Jiang, Z.H., Liu, H.Y., Wang, H.Y., Peng, J., Meersmans, J., Green, S.M., Quine, T.A., Wu, X.C., Song, Z.L., 2020. Bedrock geochemistry influences vegetation growth by regulating the regolith water holding capacity. Nat. Commun. 11, 2392. https://doi.org/10.1038/s41467-020-16156-1.

Jin, Z.Z., Qu, P.D., 1981. China's sclerophyll evergreen broad-leaved forest (in Chinese). 02, 15–22.

Jin, J.X., Zhan, W.F., Wang, Y., Gu, B.J., Wang, W.F., Jiang, H., Lu, X.H., Zhang, X.Y., 2017. Water use efficiency in response to interannual variations in flux-based photosynthetic onset in temperate deciduous broadleaf forests. Ecol. Indic. 79, 122–127. https://doi.org/10.1016/j.ecolind.2017.04.006.

Kidron, G.J., 2000. Analysis of dew precipitation in three habitats within a small arid drainage basin, Negev highlands,Israel. 55, 257–270. https://doi.org/10.1016/S0169-8095(00)00063-6.

Kljun, N., Black, T.A., Griffis, T.J., Barr, A.G., Gaumont-Guay, D., Morgenstern, K., McCaughey, J.H., Nesic, Z., 2006. Response of net ecosystem productivity of three boreal forest stands to drought. Ecosystems 9, 1128–1144. https://doi.org/10.1007/s10021-005-0082-x.

Kreft, H., Jetz, W., 2007. Global patterns and determinants of vascular plant diversity. Proc. Natl. Acad. Sci. USA 104, 5925–5930. https://doi.org/10.1073/pnas.0608361104.

Lefsky, M.A., 2010. A global forest canopy height map from the moderate resolution imaging spectroradiometer and the geoscience laser altimeter system. Geophys. Res. Lett. 37, L15401. https://doi.org/10.1029/2010GL043622.

Leuzinger, S., Zotz, G., Asshoff, R., Körner, C., 2005. Responses of deciduous forest trees to severe drought in Central Europe. Tree Physiol. 25, 641–650. https://doi.org/10.1093/treephys/25.6.641.

Li, Y., Bai, X.Y., Wang, S.J., Qin, L.Y., Tian, Y.C., Luo, G.J., 2017. Evaluating of the spatial heterogeneity of soil loss tolerance and its effects on erosion risk in the carbonate areas of southern China. Solid Earth 8, 661–669. https://doi.org/10.5194/se-8-661-2017.

Li, Q., Wang, S.J., Bai, X.Y., Luo, G.J., Song, X.Q., Tian, Y.C., Hu, Z.Y., Yang, Y.J., Tian, S.Q., 2020. Change detection of soil formation rate in space and time based on multi source data and geospatial analysis techniques. Remote Sens. 12, 1–21. https://doi.org/10.3390/rs12010121.

Liu, Z.H., Yang, J., 2014. Quantifying ecological drivers of ecosystem productivity of the early-successional boreal Larix gmelinii forest. Ecosphere 5, 84. https://doi.org/10.1890/ES13-00372.1.

Li, Y.B., Wang, S.J., Wei, C.F., Long, J., 2006. The spatial distribution of soil loss tolerance in carbonate area in Guizhou province (in Chinese). Earth Environ. 04, 36–40.

Liu, L.B., Gudmundsson, L., Hauser, M., Qin, D.H., Li, S.C., Seneviratne, S.I., 2020. Soil moisture dominates dryness stress on ecosystem production globally. Nat. Commun. 11, 4892. https://doi.org/10.1038/s41467-020-18631-1.

Lu, T.P., Zhang, W.X., Niu, J., Lin, Y.J., Wu, M.J., 2017. The vertical characteristics of soil carbon and nitrogen at different rubber plantation ages in Xishuangbanna, Southwest China (in Chinese). Fresenius Environ. Bull. 26, 1431–1439.

Marrs, R.H., Due, M.G.L., 2000. Factors controlling vegetation change in long-term experiments designed to restore heathland in Breckland,UK. 3, 135–146. https://doi.org/10.2307/1478992.

Meehl, G.A., Tebaldi, C., 2004. More intense, more frequent, and longer lasting heat waves in the 21st century. Science 305, 994–997. https://doi.org/10.1126/science.1098704.

Michael, C.W., Thomas, A.S., 2001. Influences of environment and disturbance on forest patterns in coastal Oregon watersheds. Ecology 82, 1443–1459.

Mo, J.M., Brown, S., Peng, S.L., Kong, G.H., 2003. Nitrogen availability in disturbed, rehabilitated and mature forests of tropical China. For. Ecol. Manag. 175, 573–583. https://doi.org/10.1016/S0378-1127(02)00220-7.

Montanari, A., Taqqu, M.S., Teverovsky, V., 1999. Estimating long-range dependence in the presence of periodicity: an empirical study. Math. Comput. Model. 29, 217–228. https://doi.org/10.1016/S0895-7177(99)00104-1.

Nemani, R.R., Keeling, C.D., Hashimoto, H., Jolly, W.M., Piper, S.C., Tucker, C.J., Myneni, R.B., Running, S.W., 2003. Running climate-driven increases in global terrestrial net primary production from 1982 to 1999. Science 300, 1560–1563. https://doi.org/10.1126/science.1082750.

O'Connell, C.S., Ruan, L., Silver, W.L., 2018. Drought drives rapid shifts in tropical rainforest soil biogeochemistry and greenhouse gas emissions. Nat. Commun. 9, 1348. https://doi.org/10.1038/s41467-018-03352-3.

Olson, D.M., Dinerstein, E., Wikramanayake, E.D., Burgess, N.D., Powell, G.V.N., Underwood, E.C., D'amico, J.A., Itoua, I., Strand, H.E., Morrison, J.C., Loucks, C.J., Allnutt, T.F., Ricketts, T.H., Kura, Y., Lamoreux, J.F., Wettengel, W.W., Hedao, P., Kassem, K.R., 2001]. Terrestrial ecoregions of the world: a new map of life on Earth. [dataset]Bioscience 51, 933–938. https://doi.org/10.1641/0006-3568(2001)051[0933:TEOTWA]2.0.CO;2.

Oren, R., Ellsworth, D., Johnsen, K.H., Phillips, N., Ewers, B.E., Maier, C., Schäfer, K.V.R., McCarthy, H., Hendrey, G., McNulty, S.G., Katul, G.G., 2001. Soil fertility limits carbon sequestration by forest ecosystems in a CO2-enriched atmosphere. Nature 411, 469–472. https://doi.org/10.1038/35078064.

Petrie, M.D., Wildeman, A.M., Bradford, J.B., Hubbard, R.M., Lauenrothbet, W.K., 2016. A review of precipitation and temperature control on seedling emergence and establishment for ponderosa and lodgepole pine forest regeneration. For. Ecol. Manag. 361, 328–338. https://doi.org/10.1016/j.foreco.2015.11.028.

van der Putten, W.H., Bardgett, R.D., Bever, J.D., Bezemer, T.M., Casper, B.B., Fukami, Tadashi, Kardol, P., Klironomos, J.N., Kulmatiski, A., Schweitzer, J.A., Suding, K.N., Van de Voorde, T.F.J., Wardle, D.A., 2013. Plant-soil feedbacks: the past, the present and future challenges. J. Ecol. 101, 265–276. https://doi.org/10.1111/1365-2745.12054.

Qiu, J.X., Crow, W.T., Nearing, G.S., Mo, X.G., Liu, S.X., 2014. The impact of vertical measurement depth on the information content of soil moisture times series data. Geophys. Res. Lett. 41, 4997–5004. https://doi.org/10.1002/2014GL060017.

Sankaran, M., Hanan, N.P., Scholes, R.J., Ratnam, J., Augustine, D.J., Cade, B.S., Gignoux, J., Higgins, S.I., Roux, X.L., Ludwig, F., Ardo, J., Banyikwa, F., Bronn, A., Bucini, G., Caylor, K.K., Coughenour, M.B., Diouf, A., Ekaya, W., Feral, C.J., February, E.C., Frost, P.G.H., Hiernaux, P., Hrabar, H., Metzger, K.L., Prins, H.H.T., Ringrose, S., Sea, W., Tews, J., Worden, J., Zambatis, N., 2005. Determinants of woody cover in African savannas. Nature 438, 846–849. https://doi.org/10.1038/nature04070.

Seneviratne, S.I., Corti, T., Davin, E.L., Hirschi, M., Jaeger, E.B., Lehner, I., Orlowsky, B., Teuling, A.J., 2010. Investigating soil moisture–climate interactions in a changing climate: a review. Earth-Sci. Rev. 99, 125–161. https://doi.org/10.1016/j.earscirev.2010.02.004.

Sewell, P.D., Quideau, S.A., Dyck, M., Macdonald, E., 2020. Long-term effects of harvest on boreal forest soils in relation to a remote sensing-based soil moisture index. For. Ecol. Manag. 462, 117986. https://doi.org/10.1016/j.foreco.2020.117986.

Silva, L.C.R., Lambers, H., 2018. Chapter Two–Soil–Plant–Atmosphere interactions: ecological and biogeographical considerations for climate-change research. Dev. Soil Sci. 35, 29–60. https://doi.org/10.1016/B978-0-444-63865-6.00002-8.

Simard, M., Pinto, N., Fisher, J.B., Baccini, A., 2011. Mapping forest canopy height globally with spaceborne lidar. J. Geophys. Res. 116, G04021. https://doi.org/10.1029/2011JG001708.

Stockmann, U., Minasny, B., McBratney, A.B., 2014. How fast does soil grow? Geoderma 216, 0016–7061. https://doi.org/10.1016/j.geoderma.2013.10.007.

Svenning, J.C., Kinner, D.A., Stallard, R.F., Engelbrecht, B.M.J., Wrightet, S.J., 2004. Ecological determinism in plant community structure across a tropical forest landscape. Ecology 85, 2526–2538. https://doi.org/10.1890/03-0396.

Tomsett, A.C., Toumi, R., 2001. Annual persistence in observed and modelled UK precipitation. Geophys. Res. Lett. 28, 3891–3894. https://doi.org/10.1029/2001GL013337.

Walker, B.H., Ludwig, D., Holling, C.S., Peterman, R.M., 1981. Stability of semi-arid savanna grazing systems. J. Ecol. 69, 473–498. https://doi.org/10.2307/2259679.

Walter, H., 1994. Vegetation of the earth. Third edition. Springer - Verlag, New York.

Wang, D.Z., Jiang, X., He, J.Z., Zhao, Z.H., Sun, L., Hao, H.J., 2014. Influence of simulated acid rain on transferring of cations in soils (in Chinese). Geochimica 33, 46–50. https://doi.org/10.19700/j.0379-1726.2004.01.006.

Wang, H., Liu, G., Li, Z., Zhang, L., Wang, Z., 2020a. Processes and driving insights forces for changing vegetation ecosystem services: from the Shaanxi Province of China. Ecol. Indic., 106105 https://doi.org/10.1016/j.ecolind.2020.106105.

Wang, M.J., Sun, R., Zhu, A.R., Xiao, Z.Q., 2020b. Evaluation and comparison of light use efficiency and gross primary productivity using three different approaches. Remote Sens. 12 (6), 1003. https://doi.org/10.3390/rs12061003.

Wu, B., Qi, S., 2021. Effects of underlay on hill-slope surface runoff process of Cupressus funebris Endl. plantations in Southwestern China. Forest 12 (5), 644. https://doi.org/10.3390/f12050644.

Yan, J., Zhang, Y., Yu, G., Zhou, G., Zhang, L., Li, K., Tan, Z., Sha, L., 2013. Seasonal and interannual variations in net ecosystem exchange of two old-growth forests in southern China. Agric. Ecosyst. Environ. 182–183, 257–265. https://doi.org/10.1016/j.agrformet.2013.03.002.

Yan, Y., Tian, L., Du, Z., Chang, S., Cai, Y., 2019. Carbon, nitrogen and phosphorus stocks differ among vegetation patch types in a degraded alpine steppe. J. Soils Sediments 19, 1809–1819. https://doi.org/10.1007/s11368-018-2191-0.

You, Y.M., Xu, H.C., Wu, X.P., Zhou, X.G., Tan, X.M., Li, M., Wen, Y.G., Zhu, H.G., Cai, D.X., Huang, X.M., 2020. Native broadleaf tree species stimulate topsoil nutrient transformation by changing microbial community composition and physiological function, but not biomass in subtropical plantations with low P status. For. Ecol. Manag. 477, 11849. https://doi.org/10.1016/j.foreco.2020.118491.

Yuan, D.X., 1988. On the karst enviromental system. Carsologica Sin. 7, 179.

Zhang, Z.D., Zang, R.G., 2007. Influence of ecological factors on distribution of woody plant functional types in a natural tropical forest landscape, Bawangling, Hainan island, south China (in Chinese). J. Plant Ecol. 06, 1092–1102. https://doi.org/10.17521/cjpe.2007.0137.

Zhang, Z., Jiang, H., Liu, J.X., Ju, W.M., Zhang, X.Y., 2013. Effect of heterogeneous atmospheric CO2 on simulated global carbon budget. Glob. Planet. Chang. 2013 (101), 33–51. https://doi.org/10.1016/j.gloplacha.2012.12.002.

Zhang, Y., Parazoo, N.C., Williams, A.P., Zhou, S., Gentineet, P., 2020. Large and projected strengthening moisture limitation on end-of-season photosynthesis. Proc. Natl. Acad. Sci. USA 117, 9216–9222. https://doi.org/10.1073/pnas.1914436117.

Zhang, S.R., Bai, X.Y., Zhao, C.W., Tan, Q., Luo, G.J., Wang, J.F., Li, Q., Wu, L.H., Chen, F., Li, C.J., Deng, Y.H., Yang, Y., Xi, H.P., 2021c. Global CO2 consumption by silicate rock chemical weathering: its past and future. Earth's. Future 9, e2020EF001938. https://doi.org/10.1016/j.gloplacha.2009.07.007.

Zhang, X.M., Yue, Y.M., Tong, X.W., Wang, K.L., Qi, X.K., Deng, C.X., Brandt, M., 2021a. Eco-engineering controls vegetation trends in Southwest China karst. Sci. Total Environ. 770 (8), 145160. https://doi.org/10.1016/j.scitotenv.2021.145160.

Zhang, Y.H., Xu, X.L., Li, Z.W., Xu, C.H., Luo, W., 2021b. Improvements in soil quality with vegetation succession in subtropical China karst. Sci. Total Environ. 775, 145876. https://doi.org/10.1016/j.scitotenv.2021.145876.